



AMERICAN METEOROLOGICAL SOCIETY

Journal of the Atmospheric Sciences

EARLY ONLINE RELEASE

This is a preliminary PDF of the author-produced manuscript that has been peer-reviewed and accepted for publication. Since it is being posted so soon after acceptance, it has not yet been copyedited, formatted, or processed by AMS Publications. This preliminary version of the manuscript may be downloaded, distributed, and cited, but please be aware that there will be visual differences and possibly some content differences between this version and the final published version.

The DOI for this manuscript is doi:
10.1175/2009JAS3206.1

The final published version of this manuscript will replace the preliminary version at the above DOI once it is available.



**Steady state dynamics of a density current in an f -plane
nonlinear shallow water model**

GIOVANNI A. DALU AND MARINA BALDI *

Institute of Biometeorology, Rome, Italy

* *Corresponding author address:* Marina Baldi, IBIMET-CNR, Via dei Taurini 19, 00185 Rome, Italy

E-mail: m.baldi@ibimet.cnr.it

ABSTRACT

We study the nonlinear dynamics of a density current generated by a diabatic source in a rotating and in a non-rotating system, in the presence and in the absence of frictional losses, using a steady state hydrostatic shallow water model, and producing solutions as a function of the Coriolis parameter, and of the Rayleigh friction coefficient. Results are presented in the range of the parameter values relevant for shallow atmospheric flows as sea-land breezes, and as cold pool outflows. In the shallow water approximation, single-layer flows and two-layer flows with a lid have three degrees of freedom, and their steady state dynamics are governed by three ordinary differential equations (ODE). While two-layer flows bounded by a free surface have six degrees of freedom, and their dynamics are governed by six ODEs.

We show that, in the limit case of frictionless flow, the problem has an explicit analytical solution, and that, in the presence of friction, the system for a one-layer flow and for a two-layer flow bounded by a lid can be reduced to two algebraic equations, plus one second order ordinary differential equation, which can be integrated numerically. Results show that the maximum runout length of the current occurs when the Rayleigh friction coefficient in the lower layer is of the order of the Coriolis parameter. This length is larger when the upper layer is deeper than the lower layer, but it shortens when the friction coefficient of the upper layer is smaller than that in the lower layer.

In addition, we compute the relative error of the solution to the linearized equations. This error, which is enhanced when the width of the forcing is smaller than the Rossby radius, is sizable when the friction coefficient is smaller than the Coriolis parameter. In addition, by comparing the nonlinear solution with a lid (three degrees of freedom) to the nonlinear solution with a free surface as an upper boundary (six degrees of freedom), we

show that solution with the lid overestimates the geopotential for low values of the friction coefficient, and it underestimates the geopotential for large values of this coefficient. The error, sizable when the two layers have a comparable depth, rapidly decreases when the upper layer becomes deeper than the lower layer, it results that a rigid lid can be safely adopted only when the depth of the upper layer is twice the depth of the lower layer, or deeper.

1. Introduction

We study the asymptotic behavior of density currents generated by shallow diabatic sources with a width of the order of Rossby radius as in sea-land breezes. We also study the cold pool outflows generated by narrow but intense diabatic sources, when the rotation cannot be neglected because the outflow length is comparable to the Rossby radius. While these problems are usually approached by using nonlinear numerical models (Pielke, 2002), or by linearizing the equation (Baldi et al, 2008), we use a semi-analytic nonlinear model, showing that in the shallow water approximation the behavior of these currents can be explored in a wide range of the environmental parameters with a very limited use of numerics, and producing results valuable for analyzing observed data, and simulation data of more complex nonlinear numerical models.

Density currents are driven by the gradient force due to the density difference between the intruding fluid and the ambient fluid (von Kármán, 1940). These flows are very common in nature. Examples of such flows are mesofronts, sea-land breezes, turbidity currents, fresh water intrusion in estuaries, deep water spreading on the ocean floor (Simpson, 1994). In

the absence of rotation and friction, the current propagates at a constant speed, and the runout length of the current monotonically grows in time (Huppert, 2006). The asymptotic propagation speed is $c = Fr\sqrt{g'h}$ with $Fr = O(1)$, where the Froude number, Fr , is a function of the geometry of the system, h is the depth of the density current, and g' is the reduced gravity. In a single-layer flow, when the two fluids are immiscible and frictionless, the Froude number is $Fr = \sqrt{2}$ (Benjamin, 1968). Martin and Lane-Serff (2005) have extended Benjamin's theory by including rotation and dissipation in the system.

In oceanography, reduced gravity single active layer models are still very popular (Apel 1987; Mizuta and Masuda 2003). However, mesoscale atmospheric systems have an active shallow lower layer embedded in the planetary boundary layer (PBL) where the dissipation is large, and an active deeper upper layer, which extends into the free atmosphere, where the dissipation is small (Simpson 1994; Darby et al. 2002). This makes a two-layer model approach more appropriate for atmospheric mesoscale circulations.

From an atmospheric model point of view, there are a number of recent numerical works (Seitter, 1986; Moncrieff and Liu, 1999; Liu and Moncrieff, 2000; Tompkins, 2001), and a number of analytical works, in the absence of an environment flow (Haertel et al., 2001), and in the presence of an environment flow (Xu and Moncrieff, 1994). In these model studies the Coriolis force is neglected. This can be done only when the runout length of the current is much smaller than the Rossby radius. Numerical model works, which include the Coriolis force, are those related to sea-land breeze type of flows (Segal and Arritt, 1992). This problem has been solved analytically linearizing the equations (Rotunno, 1983; Dalu and Pielke, 1989; Baldi et al., 2008).

Griffiths (1986) has shown that, in a rotating system, the Coriolis force tends to oppose

the spreading of the fluid, and that, in the absence of boundaries and of frictional losses, the flow approaches a state of geostrophic equilibrium, which inhibits any further release of potential energy. Using a lock-release technique in a non-rotating and in a rotating system, Rottman and Simpson (1983), Ungarish and Huppert (1998), Ungarish and Zemach (2003), and Hogg (2006) focus their papers on the transient from the initial state of rest towards the asymptotic state of motion. They do it theoretically, numerically, and in laboratory experiments. Their results, summarized in a paper by Huppert (2006), show that the flow undergoes through two quite different stages. During the first stage, the flow accelerates from its initial state of rest to an almost constant speed; during this transient, the effects of the frictional losses and of the Coriolis force are almost negligible. While in the second stage, the frictional losses and the Coriolis force effectively hinder the propagation of the density current. In a frictionless rotating system, the propagation of the density current stops completely when the flow is in geostrophic balance, reaching this asymptotic state in a time of the order of the inertia period. In a non-rotating system with friction, the flow progressively slows down, reaching the asymptotic state of motion in a time of the order of the inverse of the Rayleigh friction coefficient.

Since the effects of rotation and friction on the initial stage of the flow are already well documented in the literature, we focus our paper on the impact that these effects have on the shape and on the runout length of the density currents when the time is larger than inertia period and of the inverse of the Rayleigh friction coefficient. The results are presented for parameter values relevant for shallow atmospheric flows, such as those types of mesoscale circulations caused by surface sensible heat-flux gradients, when the width of the source is of the order of the Rossby radius (Segal and Arritt, 1992). The behavior of these flows is

explored in the asymptotic steady state reached when the diabatic forcing is balanced by the frictional losses and by the Coriolis force as in a Gill-Matsuno type of model (Matsuno, 1966; Gill, 1980). Our approach has the advantage that the results can be expressed in terms of readable solutions of ordinary differential equations. In fact, in the absence of friction the problem has an analytical solution. While, in the presence of friction, the system with a single-layer and with a two-layer flow bounded by a lid can be reduced to one Poisson equation plus two algebraic equations. In a two-layer flow bounded by a free surface the system can be reduced to two Poisson equations plus four algebraic equations. Since these Poisson equations can be solved with a very limited use of numerics, the behavior of the flow can be easily explored in a wide range of the parameters, summarizing the equivalent result of many numerical simulations.

In order to improve the readability of our paper, first we thoroughly examine the behavior of a current with a single active layer. This system has three degrees of freedom. Then we show that, in the presence of an upper lid, the dynamics of a two-layer flow can be reduced to a system equivalent to a single layer flow. This model is used for examining the runout length of these currents as a function of the frictional losses and of the relative depth of the two active layers, and for quantifying the amplitude of the relative error induced by linearizing the equations. Finally, we use a model with a free surface as an upper boundary and six degrees of freedom for quantifying the amplitude of the relative error induced by the rigid lid assumption.

2. Configuration and governing equations

a. Configuration

We study the dynamics of a single-layer current using an idealized one and half layer model, where the lower layer 1 is dynamically active, and where the upper layer 2 is very deep and motionless. We also study the behavior of a current with two active layers of comparable depth. This is done using a two-layer model bounded by a rigid lid placed at $z = h_1(x) + h_2(x) = \bar{H} = \text{const}$. In this case, layer 1 is $h_1(x)$ deep and its density is ρ_1 , and layer 2 is $h_2(x)$ deep and its density is ρ_2 . For completeness, we also study the behavior of this current using a two and half layer model bounded by a free surface placed at $z = H(x)$. In this case, above the free surface there is a third very deep motionless layer of fluid with density ρ_3 . \bar{H} , \bar{h}_1 , and \bar{h}_2 are the unperturbed total depth, and the unperturbed depth of the lower and intermediate layer, respectively. In atmospheric terms, the two active layers are isentropic with respective potential temperature, θ_1 and θ_2 , with above them a layer with potential temperature θ_3 (Fig. 1),

$$H = h_1 + h_2 = \bar{H} + \delta H, \quad h_1 = \bar{h}_1 + \delta h_1, \quad h_2 = \bar{h}_2 - \delta h_2, \quad \alpha = \frac{\bar{h}_1}{\bar{h}_2} = -\frac{\bar{u}_2}{\bar{u}_1} \quad (1)$$

$$\bar{\theta} = \left(\frac{\bar{h}_2 \theta_2 + \bar{h}_1 \theta_1}{\bar{H}} \right), \quad g' = g \left(\frac{\theta_2 - \theta_1}{\bar{\theta}} \right), \quad g'' = g \left(\frac{\theta_3 - \bar{\theta}}{\bar{\theta}} \right) \quad (2)$$

Static stability requires that $\rho_3 < \rho_2 < \rho_1$ ($\theta_3 > \theta_2 > \theta_1$). When $\alpha = O(1)$, the flow has two active layers, while, when $\alpha \ll 1$, only one layer is dynamically active, and the single-layer approximation can be made; u_1 and u_2 are the divergent momentum components, and

\bar{u}_1 and \bar{u}_2 are their horizontal average in the respective layers; g' is reduced gravity between layer 1 and 2, and g'' is the reduced gravity between layer 3 and layer 1 and 2. In the results shown hereafter, we assume that $g' = g'' = 10^{-2}g$, and that $\bar{h}_1 = 1$ km. In addition, in the figures, we normalize the time related variables with the inverse of the mid-latitude Coriolis parameter, $f_0 = 10^{-4} \text{ s}^{-1}$, and the space related variables with the internal Rossby radius, $R_0 = \frac{\sqrt{g'\bar{h}_1}}{f_0} = 100$ km.

b. Diabatic source

The dynamics are forced by a diabatic source. A volume $2X_Q\delta h_{0Q}$ of the fluid in layer 2 is continuously cooled from its temperature, θ_2 , down to the temperature of the lower layer, θ_1 , by a diabatic cooling source $Q(x)$,

$$\begin{cases} Q(x) = \lambda_Q\delta h_{0Q}, & \text{and } h_Q(x) = \bar{h}_1 + \delta h_{0Q}, & \text{for } 0 < |x| \leq X_Q \\ Q(x) = 0, & \text{and } h_Q(x) = \bar{h}_1, & \text{for } X_Q < |x| \leq X \end{cases} \quad (3)$$

$h_Q(x)$ is a top hat function, $2X_Q$ wide and δh_{0Q} tall (Fig. 2). In thermodynamics terms, $\tau_Q = \lambda_Q^{-1}$, is the thermal relaxation time, i.e. the decay time of the diabatic temperature perturbation; τ_Q is also the mass adjustment time as in Polvani and Sobel (2002). Throughout the paper, we take $\lambda_Q = \tau_Q^{-1} = 10^{-4} \text{ s}^{-1}$, which is the value that shifts the diurnal atmospheric mesoscale flows from noon to the early afternoon in accordance with observations (Baldi et al, 2008). In addition, we keep the volume of the perturbed fluid constant, $2X_Q\delta h_{0Q} = 0.25R_0\bar{h}_1$; i.e., in the results shown hereafter, narrow sources are deeper than

shallow wide sources, but the integrated diabatic heat has the same volume for narrow and wide sources.

c. Governing equations

Posing that $\partial_y \equiv 0$, the steady state dynamics of a two-layer flow are governed by the following six 1st Ordinary Differential Equations (ODEs),

$$\left\{ \begin{array}{l} D_x[h_1(x) u_1(x)] = \lambda_Q [\delta h_Q(x) - \delta h_1(x)] \\ \\ \lambda_1 u_1(x) + u_1(x) D_x u_1(x) + g' D_x h_1(x) + g'' D_x H(x) - f v_1(x) = 0 \\ \\ \lambda_1 v_1(x) + u_1(x) D_x v_1(x) + f u_1(x) = 0 \\ \\ D_x \{[h_2(x) u_2(x)]\} = -\lambda_Q [\delta h_Q(x) + \delta h_2(x)] \\ \\ \lambda_2 u_2(x) + u_2(x) D_x u_2(x) + g'' D_x H(x) - f v_2(x) = 0 \\ \\ \lambda_2 v_2(x) + u_2(x) D_x v_2(x) + f u_2(x) = 0 \end{array} \right. \quad (4)$$

The system has six degrees of freedom, because the barotropic mode is not independent. In fact, since $H(x) = h_1(x) + h_2(x)$, the equation for this mode is yielded by the sum of the 1st equation with the 4th equation,

$$D_x [h_1(x)u_1(x) + h_2(x)u_2(x)] = -\lambda_Q \delta H(x) = -\lambda_Q [H(x) - \bar{H}] \quad (5)$$

In equations (4), the 1st equation is the mass balance in layer 1, and the 4th equation is the mass balance in layer 2. The other four equations are the momentum equations, where $u_i(x)$ and $v_i(x)$ for $i = (1, 2)$ are the divergent and the rotational momentum components in the respective layers, $g'D_x h_1(x)$ is the gradient force associated to the diabatic source, and $g''D_x H(x)$ is the gradient force due to the deformation of the upper free surface. The dynamics are driven by the buoyancy force generated by a diabatic source confined around the origin. This source forces an increase of depth of $h_1(x)$ equal to $\delta h_Q(x) = \delta h_{0Q}$ for $0 < |x| \leq X_Q$, and equal to $\delta h_Q(x) = 0$ for $X_Q < |x| \leq X$; it results that $h_Q(x) = \bar{h}_1 + \delta h_{0Q}$ for $0 < |x| \leq X_Q$, and $h_Q(x) = \bar{h}_1$ for $X_Q < |x| \leq X$. The perturbation propagates away from the source region as a bore; the spreading of the fluid is opposed by the Coriolis force, inertia, and frictional losses, limiting the runout length of the diabatically perturbed fluid (Fig. 2).

In equations (4), it has been assumed that the dynamics are steady, $\partial_t \equiv 0$, this is when the time t is sufficiently larger than the inertial period and of the other time scales of the flow, $t \gg (f^{-1}, \tau_Q, \lambda_1^{-1}, \lambda_2^{-1})$. In layer 1, the frictional losses are due to the interaction of the current with the rough terrain. These losses are parameterized by the Rayleigh friction coefficient, λ_1 . The relation between λ_1 and the drag coefficient, C_D , is $\lambda_1 = \left(\frac{fK}{2\bar{h}_1^2}\right)^{\frac{1}{2}}$ with $2\bar{u}_1 C_D = \left(\frac{fK}{2}\right)^{\frac{1}{2}}$, where K is the diffusion coefficient in the Ekman layer (Gill, 1982). In layer 2, the losses are due to the friction between the current and the ambient flow. These losses are parameterized by λ_2 . In shallow atmospheric flows $\lambda_2 \leq \lambda_1$. In addition, since

the Boussinesq approximation has been made, it is assumed that $\delta\rho \ll \bar{\rho}$ (Gill, 1982; Pedlosky, 1987). In equations (4), it has been assumed that the Reynolds number is large, $Re = \left(\frac{u_1 h_1}{K}\right) \gg 1$, and that the flow is unsheared (Huppert, 2006). The shallow water approach demands that the aspect ratio $A = \left(\frac{H}{2X}\right) \ll 1$, where $2X$ and H are the width and the depth of the flow, respectively.

In a non-rotating system, where denser fluid intrudes into the lighter fluid through the entire depth of layer 1, a steep interface separates the two fluids at the frontal edge of the current; in this region a strong deep overturning can even block the upstream inflow (Moncrieff and So, 1989). Also in a rotating system a complex internal circulation can develop within the current (Martin et al, 2005). When these internal circulations become important in shaping the flow, the adoption of the shallow water approximation is ruled out.

In our model, the layers have an average prescribed finite depth, and the active layers are separated by a relatively smooth interface (Fig. 1). The diabatically perturbed heavier fluid in layer 1 intrudes into the lighter fluid of layer 2. The leading edge of this perturbation does not show a steep frontal zone like in the classical density currents (Moncrieff and So, 1989), but it is more like a shallow wedge (Fig. 2), as a consequence the shallow water approximation holds also at the edges of the flow.

3. Dynamics in a single-layer flow

Since in a single-layer flow the ambient fluid above the current is motionless, the dynamics are governed by the first three equations in (4). Taking advantage of this simplification, we develop a method for computing the nonlinear solution to this problem. We also explore

the limit of the linear solution for different values of the environment parameters, and for different geometries of the source. In following sections, we upgrade the method to the two-layer flow with a lid, and to the two-layer flow with a free surface.

a. Numerical nonlinear solution in the presence of friction

Since $h_Q(x)$ is an even function, $h_1(x)$ is also an even function. The flow is confined within the region where $|x| \leq X$, with no flow through the edges [$u_1(-X) = u_1(X) = 0$]; the width of the flow, $2X$, is computed by integrating the 1st equation in (4),

$$\int_{-X}^X D_x[h(x) u_1(x)] dx = 0 \Rightarrow \int_{-X}^X h_Q(x) dx = \int_{-X}^X h(x) dx \quad (6)$$

Since $\delta h_1(|x| > X) = 0$, X is the runout length of the flow, the region where $|x| \leq X_Q$ is the source region, and the region where $X_Q < |x| \leq X$ is the outflow region.

By inspection of the 1st equation in (4), it can be deduced that in the source region the flow is divergent, while in the outflow region the flow is convergent. Taking advantage of this property, Polvani and Sobel (2002) have studied the dynamics of these currents by assuming that the divergent momentum component is piecewise linear, with constant divergence in the source region and constant convergence in the outflow region. In addition, they have assumed that the envelope of the current is flat. In geophysics, this is the weak temperature gradient approximation, WTG (Sobel and Bretherton, 2000; Sobel et al, 2001). In fluid dynamics, models with flat interface are called box models (Huppert and Simpson, 1980).

In our study, the shape of the envelope, $h_1(x)$, is not prescribed *a priori*, but it is computed by solving the Poisson equation obtained by taking the x -derivative of the 2nd

equation in (4), with $g'' D_x H(x) \equiv 0$,

$$D_{xx}h_1(x) = \frac{1}{g'} \left[f\zeta_1(x) - \lambda_1\delta_1(x) - \frac{1}{2}D_{xx}u_1^2(x) \right], \text{ with } D_x u_1 = \delta_1, \text{ and } D_x v_1 = \zeta_1 \quad (7)$$

Then $h_1(x)$ is computed in finite differences by dividing the width of the flow, $2X$, in $N = 2^n$ intervals $I_n \equiv (x_n, x_{n+1})$, $\Delta x = \left(\frac{2X}{N}\right)$ long, and by taking the divergent momentum component piecewise linear within each of these intervals, $[D_x u_1 = \bar{\delta}_1]_{x \in I_n}$,

$$h_{1,n+1} - 2h_{1,n} + h_{1,n-1} = \frac{\Delta x^2}{g'} \left[f\bar{\zeta}_{1,n} - \lambda_1\bar{\delta}_{1,n} - \bar{\delta}_{1,n}^2 - \frac{u_{1,n}(\bar{\delta}_{1,n+1} - \bar{\delta}_{1,n-1})}{2\Delta x} \right] \quad (8)$$

$h_{1,n}$ is computed by cyclic reduction, posing $h_1(-X) = h_1(X) = \bar{h}_1$ at the edges of flow. The required accuracy of the solution is achieved by increasing N ; hereafter, we take N equal to 2^{10} . The runout length, $X = \left(\frac{N}{2}\right) \Delta x$, is computed by setting Δx equal to the value for which X balances the equation in (6). In Eq. (8), the terms, $\bar{\delta}_{1,n}$ and $\bar{\zeta}_{1,n}$, are yielded by the solution to the 1st equation in (4) and to the 3rd equation in (4), respectively. Assuming that the divergent momentum component is piecewise linear, the 1st equation in (4) yields

$$D_x h_1(x) + \frac{(\lambda_Q + \bar{\delta}_{1,n})}{\bar{\delta}_{1,n}x} h_1(x) = \frac{\lambda_Q h_Q(x)}{\bar{\delta}_{1,n}x} \Rightarrow h_1(x) = \frac{\lambda_Q h_Q(x)}{\lambda_Q + \bar{\delta}_{1,n}}, \text{ for } x \in I_n \quad (9)$$

Then $\bar{\delta}_{1,n} = \lambda_Q \left(\frac{h_{Qn} - h_{1,n}}{h_{1,n}}\right)$, this algebraic equation, solution to the ODE in (9), states that within each of the intervals the divergence is proportional to the difference between the depth of the forcing and the profile of the interface, and that the proportionality constant is the inverse of the mass adjustment time. Small values of λ_Q lead to a small divergence, $\bar{\delta}_{1,n}$, and a short runout length, X ; while large values of λ_Q lead to a large divergence and runout

length. The vorticity equation, obtained by taking the x -derivative of the 3rd equation in (4), yields,

$$\lambda_1 \zeta_1 + D_x [u_1(\zeta_1 + f)] = 0 \Rightarrow D_x \zeta_1 + \frac{(\bar{\delta}_{1,n} + \lambda_1)\zeta_1}{\bar{\delta}_{1,n}x} = -\frac{f}{x} \Rightarrow \bar{\zeta}_{1,n} = -\frac{\bar{\delta}_{1,n}f}{\bar{\delta}_{1,n} + \lambda_1} \quad (10)$$

The vorticity, $\bar{\zeta}_{1,n}$, is a function of the mass adjustment time, λ_Q^{-1} , through the divergence, $\bar{\delta}_{1,n}$. In addition, the algebraic equation, solution to the vorticity equation in (10), states that where the divergence is constant the vorticity is also constant. Note that $\bar{\delta}_{1,n}$ and $\bar{\zeta}_{1,n}$ are constant for $x \in I_n$, but they can assume different values in different intervals. The momentum component, $u_1(x)$, is computed by cyclic reduction of $D_{xx}u_1(x) = D_x\delta_1(x)$, posing $u_1(x = X) = u_1(x = -X) = 0$. The envelope of the current is shown in Fig. 2.

The solution to the first order ODEs (Eq.s 9-10) has been constructed using a mathematical handbook (Zwillinger, 1992). The numerical solution to the Poisson equation has been computed by cyclic reduction following the method shown by Potter (1973).

Finally, the position $\partial_y \equiv 0$ can be relaxed by posing that the divergence and the vorticity are constant within each of the 2-D grid element, i.e. the behavior of a density current in the (x, y) -plane can be studied by computing the solution to a 2-D Poisson equation; in this paper we do not further elaborate on this extension of our theory.

b. Nonlinear solution in the absence of friction

When the final state of the flow is non divergent and in geostrophic balance, the problem has an analytical explicit solution. The profile of the interface, $h_1(x)$, is computed as following, Eq. (10) yields the vorticity, $\zeta_1 = D_x v_1(x) = -f$, which integrated yields $v_1(x) = -fx$,

having posed $v_1(0) = 0$. Then the slope of the interface, $D_x h_1(x)$, is yielded by the 2nd equation in (4), which integrated, posing $h_1(-X) = h_1(X) = \bar{h}_1$, yields $\delta h_1(x)$, finally, the width of the flows is computed imposing the mass balance (Eq. 6).

$$D_x \delta h_1(x) = -\frac{f^2 x}{g'}, \quad \delta h_1(x) = \frac{f^2 (X^2 - x^2)}{2g'}, \quad X = \left[\frac{3g'(\delta h_{0Q} X_Q)}{f^2} \right]^{\frac{1}{3}} \quad (11)$$

The envelope of a current in geostrophic balance is parabolic (Fig. 2). Its shape does not depend on the shape of the source. The runout length, X , does not depend on the shape of the source, but only on the volume of the diabatically perturbed fluid.

In the absence of friction and in the absence of rotation, $\lambda_1 = f = 0$, the integral of the 2nd equation in (4) yields the propagation speed of the density current,

$$c^2 = u_1^2(X) = 2g' [h_1(0) - h_1(X)] \Rightarrow c = u_1(X) = Fr \sqrt{g' \Delta h_1}, \quad \text{with } Fr = \sqrt{2} \quad (12)$$

When $\Delta h_1 = [h_1(0) - h_1(X)] \rightarrow \bar{h}_1$, then $c \rightarrow \sqrt{2g'\bar{h}_1}$ and the propagation speed of the current is as in Benjamin (1968). When the flow is divergent and frictionless, the integral of the 2nd equation in (4) yields that the runout length of a current in a rotating system equals the propagation speed in a non-rotating system multiplied by the inertia period,

$$\int_0^X D_x \left[g' \delta h_1(x) + \frac{1}{2} u_1^2(x) \right] dx = -\frac{1}{2} f^2 X^2 \Rightarrow X = \left(\frac{c}{f} \right) \quad (13)$$

In the above integral, it has been assumed that $u_1(0) = u_1(X) = 0$, and that $\Delta h_1 = \delta h_1(0) - \delta h_1(X)$ with $\delta h_1(X) = 0$. When $\Delta h_1 \rightarrow \bar{h}_1$, $X \rightarrow \sqrt{2} R_0$, and the runout length is of the order of the Rossby radius.

c. Linear solution in the presence of friction

Linear models are still used for studying the behavior of sea-land breeze flows (Rotunno, 1983; Dalu and Pielke, 1993; Baldi et al, 2008), therefore, it is important to explore the validity of these models. A manipulation of the linear expansion of the first three equations in (4) yields the following second order equation for $h_1(x)$,

$$D_{xx}h_1 + \nu^2 h_1 = -\nu^2 h_Q, \text{ with } \nu^2 = \frac{\lambda_Q \lambda_D}{g' \bar{h}_1}, \text{ and } \lambda_D = \frac{\lambda_1^2 + f^2}{\lambda_1} \quad (14)$$

The solution to Eq. (14) is computed as a convolution of the Green function with the inhomogeneous term,

$$\delta h_1(x) = -\nu^2 \{g(x, \xi) * \delta h_Q(\xi)\}, \text{ with } g(x, \xi) = -\frac{\exp(-\nu|x-\xi|)}{2\nu}$$

$$\delta h_1(x) = \delta h_{0Q} \begin{cases} [1 - \exp(-\nu X_Q) \cosh(\nu x)], \text{ for } |x| \leq X_Q \\ \sinh(\nu X_Q) \exp(-\nu|x|), \text{ for } |x| > X_Q \end{cases} \quad (15)$$

ν^{-1} is the e -folding distance of $\delta h_1(x)$ in the outflow region. Since in a non-rotating system $\nu \propto \sqrt{\frac{\lambda_1}{\tau_Q}}$, the aspect ratio of the flow monotonically decreases as the Rayleigh friction coefficient increases, and as the mass adjustment time decreases. Since in a rotating system $\nu \propto \sqrt{\frac{\lambda_1^2 + f^2}{\lambda_1}}$, the aspect ratio of the flow is smallest when $\lambda_1 = f$. The range of validity of the linear solution is evaluated by computing the geopotential relative error,

$$\epsilon_{linear} = \left[\frac{\Delta h_{1linear} - \Delta h_{1nonlinear}}{\Delta h_{1nonlinear}} \right] \quad (16)$$

With $\Delta h_1 = \delta h_1(x = 0)$, where $\Delta h_{1_{linear}}$ is computed by using Eq. (15), and $\Delta h_{1_{nonlinear}}$ is computed by using Eq. (8). Results show that the linear solution overestimates the geopotential at low values of the Rayleigh friction coefficient, and it underestimates the geopotential at intermediate and large values of the friction coefficient. The error is sizable only when the frictional losses are weak (Fig. 3). In addition, this error is very large when the diabatic source is narrow and deep (Fig. 4). This behavior is due to the fact that the linear approximation holds when $\lambda_1 u_1 \gg u_1 D_x u_1$ and $\lambda_1 v_1 \gg u_1 D_x v_1$. Since $v_1 \propto u_1$ in the linear solution, this approximation holds when $\lambda_1 \gg D_x u_1 = \bar{\delta}_1 = \lambda_Q \frac{(h_Q - h_1)}{h_1}$, this is when $(h_Q - h_1) \ll h_1$, i.e. for wide shallow forcing.

When $\nu X_Q \ll 1$, a Taylor expansion of the exponential in Eq. (15) yields $\delta h_1(x = 0) = \nu X_Q \delta h_{0Q}$. In a non-rotating system, $\delta h_1(x = 0) = \sqrt{\frac{\lambda_Q \lambda_1}{g' h_1}} (\delta h_{0Q} X_Q) \rightarrow 0$ when $\lambda_1 \rightarrow 0$, and, in a rotating system, $\delta h_1(x = 0) = \left[\sqrt{\frac{\lambda_Q (\lambda_1^2 + f^2)}{f \lambda_1}} \left(\frac{X_Q}{R_0} \right) \right] \delta h_{0Q} \rightarrow \infty$ when $\lambda_1 \rightarrow 0$. Therefore, when λ_1 is small, the geopotential near the origin is overestimated for $f \neq 0$, while it is underestimated for $f = 0$. In a following section, it will be shown that this behavior is due to the absence in the linear solution of the divergent quadratic terms, which become dominant in the nonlinear solution when λ_1 is small.

Summarizing the results shown in Figs (3-4), we can conclude that the linear approximation is generally valid when the width of the source is comparable with the Rossby radius, and when the Rayleigh friction coefficient is comparable to the Coriolis parameter. While, the linear approximation is not generally valid for currents generated by narrow deep sources, as atmospheric downdrafts forced by evaporation of precipitation (Fujita, 1959).

The solution to the linear second order ODE has been constructed using a mathematical handbook (Zwillinger, 1992).

4. Dynamics in a two-layer flow bounded by a rigid lid

Shallow atmospheric flows are usually bounded by a temperature inversion, which decouples the mesoscale circulation from the free atmosphere above it. In models this inversion is often parameterized by adopting a lid as an upper boundary (Pielke, 2002). Therefore, in this section we analyze the dynamics of a two-layer flow bounded by a lid. The validity of this upper boundary condition will be discussed in a following section.

a. Lid reaction

Rottman and Simpson (1983) have shown that, in a non-rotating system, a two-layer flow bounded by a lid has two degrees of freedom. We show that, in a rotating system, these flows have three degrees of freedom, and that their dynamics are governed by a set of three ODEs, equivalent to those of a single-layer flow. In fact, in the presence of a lid, $\delta H(x) = 0$, and in the absence of flow through the edges, $[u_1(-X) = u_1(X) = u_2(-X) = u_2(X) = 0]$, Eq. (5) yields,

$$h_1(x)u_1(x) + h_2(x)u_2(x) = 0 \Rightarrow u_2(x) = -\frac{h_1(x)}{h_2(x)}u_1(x) \approx -\alpha u_1(x) \quad (17)$$

The approximation in the last equation establishes an algebraic relation between $u_1(x)$ and $u_2(x)$. In addition, the role of $g'' D_x H(x)$ in the 2nd and 5th equation in (4) is taken by lid reaction. Assuming that this reaction is proportional to gradient force, $D_x \phi \propto g' D_x h_1$, we evaluate the proportionality constant by taking the ratio between the 5th equation and the 2nd equation in (4),

$$D_x \phi = -\mu g' D_x h_1, \quad \text{with } \mu = \frac{\beta}{1 + \beta}, \quad \text{and } \beta = \alpha \left[\frac{\lambda_1(\lambda_2^2 + f^2)}{\lambda_2(\lambda_1^2 + f^2)} \right] \quad (18)$$

In the construction of the equation for the lid reaction (1st Eq. in 18), the nonlinear terms in the 3rd and the 6th equations in (4) having been neglected. We recall that when $\alpha = 0$ ($h_2 = \infty$), only the lower layer is active, the lid reaction vanishes, and the driving gradient force is as in a single-layer flow. In a non-rotating system β equals α , then μ equals $\frac{\alpha}{1+\alpha}$. When $h_1 = h_2$ ($\alpha = 1$), the lid reaction accounts for half of the driving gradient force, $\mu = \frac{1}{2}$.

b. Numerical nonlinear solution for a two layer-flow with friction and a lid

When Eq. (18) holds, the gradient force reduces to $(1 - \mu)g'D_x h_1(x)$ in the 2nd Eq. (4), and the dynamics are governed by the first three equations in (4), consequently the presence of a lid greatly simplifies the dynamics by halving the degrees of freedom. The validity of this solution is discussed in a following section.

The envelope of the current, $h_1(x)$, is computed by cyclic reduction as in a single-layer flow (Eq. 8), with $\bar{\delta}_{1,n}$ and $\bar{\zeta}_{1,n}$ as in Eq.s (9-10),

$$h_{1,n+1} - 2h_{1,n} + h_{1,n-1} = \frac{\Delta x^2}{g'} \left[\frac{f\bar{\zeta}_{1,n} - \lambda_1\bar{\delta}_{1,n} - \bar{\delta}_{1,n}^2}{1 - \mu} - \frac{u_{1,n}(\bar{\delta}_{1,n+1} - \bar{\delta}_{1,n-1})}{2\Delta x(1 - \mu)} \right] \quad (19)$$

The runout length, X , is computed by using Eq. (6). Results show that this length is smaller when the friction coefficient in the upper layer is smaller than the friction coefficient in the lower layer. In addition, this length grows for increasing depth of the upper layer (decreasing values of α), and for increasing values of friction coefficient of lower layer, up to a value of

this coefficient of the order Coriolis parameter, to decrease thereafter. When λ_2/λ_1 is a fraction smaller than unity, the maximum value of the outflow distance shifts to values of λ_1/f_0 larger than unity (Fig. 5).

c. Linear solution for a two layer-flow with friction and a lid

The linear solution for a two layer flow with a lid is formally as in equation (15), but with the following wavenumber,

$$\nu = \sqrt{\frac{\lambda_Q \lambda_D}{g' h_1 (1 - \mu)}}, \quad \text{with } \lambda_D = \frac{\lambda_1^2 + f^2}{\lambda_1}, \quad \text{and } \mu(\alpha, f, \lambda_1, \lambda_2) \text{ as in Eq. (18),} \quad (20)$$

The inverse of this wavenumber, ν^{-1} , is the e -folding distance for $h_1(x \geq X_Q)$. The isopleths in Fig. 6 show that this distance grows for increasing depth of layer 2, and for increasing values of λ_1 up to $\lambda_1 = f_0$ when $\lambda_2 = \lambda_1$, to decrease thereafter. When λ_2/λ_1 is a fraction smaller than unity, the maximum value of this distance shifts to values of λ_1/f_0 larger than unity, as in the nonlinear solution shown in Fig. 5. Note that, within the validity limits of the linear solution, ν^{-1} is a valuable parameter, because it does not depend on the shape or on the intensity of the source. In Fig. 6 the isopleths for $\lambda_1 < 0.1 f_0$ are not shown, because the linear solution fails when the frictional losses are small. The relative error in a two-layer flow with a lid is as that in a single-layer flow (Fig.s 3-4).

d. Explicit nonlinear solution with friction and a lid

With Eq. (19) we have shown how a high resolution solution for $h_1(x)$ can be computed numerically. In this section we show that an explicit approximate nonlinear solution for $h_1(x)$ can be constructed by posing that $u_1(x)$ is piecewise linear in the source region and in the outflow region,

$$\bar{\delta}_{1,1} = \lambda_Q \frac{X - X_Q}{X_Q}, \quad \bar{\delta}_{1,2} = -\lambda_Q, \quad \bar{\zeta}_{1,1} = -f \frac{\bar{\delta}_{1,1}}{\bar{\delta}_{1,1} + \lambda_1}, \quad \bar{\zeta}_{1,2} = -f \frac{\bar{\delta}_{1,2}}{\bar{\delta}_{1,2} + \lambda_1}$$

Then, replacing $g' D_x h_1(x) + g'' D_x H(x)$ with $g'(1 - \mu) D_x h_1(x)$ in the 2nd equation in (4), the integral $\int_x^X D_{x'} [g'(1 - \mu) \delta h_1(x') + \frac{1}{2} u_1^2(x')] dx'$ yields,

$$\delta h_1(x) = \begin{cases} \frac{(\lambda_1 \bar{\delta}_{1,2} - f \bar{\zeta}_{1,2})(X - X_Q)^2 + (\lambda_1 \bar{\delta}_{1,1} - f \bar{\zeta}_{1,1})(X_Q^2 - x^2) - \bar{\delta}_{1,1}^2 x^2}{2g'(1 - \mu)}, & \text{for } 0 \leq |x| < X_Q \\ \frac{(\lambda_1 \bar{\delta}_{1,2} - f \bar{\zeta}_{1,2})[(X - X_Q)^2 - (|x| - X_Q)^2] - [\bar{\delta}_{1,1} X_Q + \bar{\delta}_{1,2} (|x| - X_Q)]^2}{2g'(1 - \mu)}, & \text{for } X_Q \leq |x| \leq X \end{cases} \quad (21)$$

A Taylor expansion of the linear solution in Eq. (15) shows that the linear solution captures the main characteristics of the nonlinear solution with friction in Eq. (21). In fact this expansion shows that $\delta h_1(x)$ has a quadratic term in the source region and a linear term in the outflow region as the solution in Eq. (21). But, while the linear solution keeps the same structure when the frictional losses are small, for small frictional losses the linear term becomes negligible in the nonlinear solution, while the quadratic terms related to the divergence (which are absent in the linear solution) become dominant. This dominance is very evident in the limit case of the frictionless nonlinear solution,

$$\delta h_1(x) = \frac{1 + \alpha}{2g'} \begin{cases} f^2 [(X - X_Q)^2 + (X_Q^2 - x^2)] - \bar{\delta}_{1,1}^2 x^2, & \text{for } 0 \leq |x| < X_Q \\ f^2 [(X - X_Q)^2 - (|x| - X_Q)^2] - [\bar{\delta}_{1,1} X_Q + \bar{\delta}_{1,2} (|x| - X_Q)]^2, & \\ & \text{for } X_Q \leq |x| \leq X \end{cases} \quad (22)$$

Where X in Eq. (21) and in Eq. (22) is the positive root of the third order algebraic equation obtained by posing, in the respective equations, $\int_{-X}^X h_1(x') dx' = 2\delta h_{0_Q} X_Q$. In a frictionless rotating system, $X = \frac{c}{f}$, where c is the propagation speed in a non rotating system; c is as in a single layer flow (Eq. 12), but with $Fr = \sqrt{\frac{2}{1+\alpha}}$. When $\alpha = 1$ and $\delta h_1 = \bar{h}_1$, $X = R_0$, the runout length is equal to the Rossby radius.

5. Two-layer flow bounded by a free surface

We have shown that the adoption of a lid as an upper boundary halves the degrees of freedom simplifying the dynamics of the system. In order to analyze the range of validity of this simplification for shallow atmospheric flows, we compare the solution with a lid with the solution with a free surface as an upper boundary. This last system has six degrees of freedom, and its dynamics are governed by the six ODEs in (4).

a. Numerical nonlinear solution for a two layer-flow with friction and a free surface

The 5th equation in (4) yields the slope of the free surface, and the difference between this equation and the 2nd equation (4) yields the slope of the interface,

$$\left\{ \begin{array}{l} D_x H = \frac{1}{g'} (f v_2 - \lambda_2 u_2 - u_2 D_x u_2), \text{ with } h_2 = H - h_1 \\ D_x h_1 = -\frac{1}{g'} [f (v_2 - v_1) + (\lambda_1 u_1 - \lambda_2 u_2) + u_1 D_x u_1 - u_2 D_x u_2] \end{array} \right. \quad (23)$$

H and h_1 are computed by cyclic reduction of the two Poisson equations obtained by taking the x -derivative of the two equations in Eq. (23), posing $u_1=u_2=0$, $h_1 = \bar{h}_1$ and $H = \bar{H}$ at the two edges of the flow,

$$\left\{ \begin{array}{l} H_{n+1} - 2H_n + H_{n-1} = \frac{\Delta x^2}{g'} [f \bar{\zeta}_{2,n} - \lambda_2 \bar{\delta}_{2,n} - \bar{\delta}_{2,n}^2 - \frac{u_{2,n}}{2\Delta x} (\bar{\delta}_{2,n+1} - \bar{\delta}_{2,n-1})] \\ h_{1,n+1} - 2h_{1,n} + h_{1,n-1} = \frac{\Delta x^2}{g'} \{ [f \bar{\zeta}_{1,n} - \lambda_1 \bar{\delta}_{1,n} - \bar{\delta}_{1,n}^2 - \frac{u_{1,n}}{2\Delta x} (\bar{\delta}_{1,n+1} - \bar{\delta}_{1,n-1})] \\ \quad - [f \bar{\zeta}_{2,n} - \lambda_2 \bar{\delta}_{2,n} - \bar{\delta}_{2,n}^2 - \frac{u_{2,n}}{2\Delta x} (\bar{\delta}_{2,n+1} - \bar{\delta}_{2,n-1})] \} \end{array} \right. \quad (24)$$

$$\bar{\delta}_{1,n} = \lambda_Q \left(\frac{h_{Q_n} - h_{1,n}}{h_{1,n}} \right), \quad \bar{\delta}_{2,n} = -\lambda_Q \left(\frac{h_{Q_n} + h_{2,n}}{h_{2,n}} \right), \quad \bar{\zeta}_{1,n} = -\frac{\bar{\delta}_{1,n} f}{\bar{\delta}_{1,n} + \lambda_1}, \quad \bar{\zeta}_{2,n} = -\frac{\bar{\delta}_{2,n} f}{\bar{\delta}_{2,n} + \lambda_2}$$

The range of validity of the solution with a lid is evaluated by computing the geopotential relative error,

$$\epsilon_{lid} = \left[\frac{\Delta h_{1lid} - \Delta h_{1free}}{\Delta h_{1free}} \right] \quad (25)$$

With $\Delta h_1 = \delta h_1(x = 0)$, where Δh_{1lid} is computed by using Eq. (19), and Δh_{1free} is computed by using Eq. (24). The rigid lid solution overestimates the geopotential at low values of the friction coefficient, and it underestimates the geopotential at high values of this coefficient, this behavior is enhanced by small frictional losses in the upper layer (Fig. 7).

The error decreases as the depth of the upper layer increases, and it becomes negligible when $\alpha \ll 1$. But the error is always sizable when the two active layers have a comparable depth, $\alpha \approx 1$. The rigid lid upper boundary can be safely adopted in those shallow atmospheric two-layer flow models where the upper layer is sufficiently deeper than the lower layer, this is when the depth of the upper layer is twice the depth of the lower layer, or deeper ($\alpha < 0.5$ in Fig. 7).

Note that the method used for constructing the solution for two-layers can be easily extended to a stack of layers, i.e. a multilayer nonlinear model can be constructed by piling up a number of shallow layers.

b. Frictionless two-layer flow with a free surface

When the flow is non-divergent and in geostrophic balance, the 3rd and the 6th equations in (4), with $\lambda_1 = \lambda_2 = 0$, but $f \neq 0$ and $\alpha \neq 0$, yield,

$$v_1(x) = -fx \text{ and } v_2(x) = f(X - x), \text{ with } v_1(0) = v_2(X) = 0 \quad (26)$$

The difference between the 5th and the 2nd equation in (4) yields the slope of $h_1(x)$, $D_x h_1 = \frac{f}{g'}(v_1 - v_2)$, which integrated, imposing that $[\delta h_1(-X), \delta h_1(X)] = (0, 0)$, yields $\delta h_1(x)$, then the width of the flow is computed imposing the mass balance as in the single-layer flow (Eq. 6).

$$D_x \delta h_1(x) = -\frac{f^2 X}{g'}, \quad \delta h_1(x) = \frac{f^2 X (X - |x|)}{g'}, \quad X = \left[\frac{2g'(\delta h_{0Q} X_Q)}{f^2} \right]^{\frac{1}{3}} \quad (27)$$

In a two-layer flow in geostrophic balance, the width of the flow, $2X$, is insensitive to the shape of the diabatic forcing and to the relative depth of the two layers, α ; the slope of the envelope of the current is constant (Fig. 8).

An explicit nonlinear solution for a two-layer flow with a free surface can be constructed by posing that the divergence is a piecewise linear in the source and in the outflow region,

$$g'' \delta H(x) = -\frac{1}{2}f^2(X - |x|)^2 - \frac{1}{2}\alpha^2 \begin{cases} \bar{\delta}_{1,1}^2 x^2, & \text{for } 0 \leq |x| < X_Q \\ \bar{\delta}_{1,2}^2 (X - |x|)^2, & \text{for } X_Q \leq |x| \leq X \end{cases} \quad (28)$$

$$g' \delta h_1(x) = f^2 X (X - |x|) - \frac{1}{2}(1 - \alpha^2) \begin{cases} \bar{\delta}_{1,1}^2 x^2, & \text{for } 0 \leq |x| < X_Q \\ \bar{\delta}_{1,2}^2 (X - |x|)^2, & \text{for } X_Q \leq |x| \leq X \end{cases} \quad (29)$$

The runout length of the current X is the positive root of the following third order algebraic equation,

$$\frac{f^2}{2g'} X^3 - \frac{\lambda_Q^2 (1 - \alpha^2)}{6g'} X (X - X_Q)^2 = \delta h_{0_Q} X_Q \quad (30)$$

It is often said that, in a rotating system, the final state of a non-dissipative density current is in geostrophic balance. Thomas and Linden (2007) find a reasonable good agreement between observed flows in rotating tank experiments and a simple geostrophic theory. However, this is not always the case, for instance, in the presence of a coastal boundary, the kinematic requirement of zero flow across the right boundary in the northern hemisphere removes the component of the Coriolis force, breaking the geostrophic balance. It results that

the ageostrophic component of the flow in the head region becomes important in shaping the current (Hacker and Linden, 2002).

Our geostrophic solution is independent from the relative depth of the two fluids and from the shape of the source (Eq. 27). But, even a tiny amount of ageostrophy completely changes its behavior, making the shape of the interface dependent on the relative depth of the two fluids and on the shape of the source (Eq. 29). In an initial value problem, the ageostrophic transient may favor the ageostrophic solution in Eq. (29) for the asymptotic state of the flow. However, note that, when the two layers have an equal depth ($\alpha = 1$), the runout length of the divergent non-dissipative flow and the shape of the interface are equal to those of a current in geostrophic balance (see Eq.s 27, 29, and 30). It follows that the geostrophic balance solution is appropriate for the asymptotic state when $\alpha \approx 1$, i.e. in a two-layer flow with fluids of comparable depth.

6. Conclusions

Using a nonlinear shallow water model with two isentropic layers, and with three isentropic layers, we have studied the asymptotic behavior of density currents generated by a diabatic source with different upper boundary conditions, and for different values of the environment parameters.

We have shown that the behavior of these currents can be explored in a wide range of the environmental parameters with a very limited use of numerics. In fact, in a single-layer shallow water approximation, and in a two-layer shallow water approximation with a lid, a high resolution solution can be obtained using two algebraic equations and a Poisson

equation. In a two-layer shallow water approximation with a free surface, a high resolution solution can be obtained using four algebraic equations and two Poisson equations.

We also have shown that, in the limit case of frictionless flows, the problem has an explicit analytical solution. An explicit approximate nonlinear solution can be obtained for flows with friction by assuming that the momentum divergent component is piecewise linear in the source region and in the outflow region.

Using these models, we have shown that the maximum runout length of the current occurs when the Rayleigh friction coefficient in the lower layer is of the order of the Coriolis parameter. This maximum runout length is shorter when the Rayleigh friction coefficient of the upper layer is smaller than that of the lower layer. While, for a given distribution of the frictional losses, it is larger when the upper layer is deeper.

In addition, we have shown that the solution to the linearized equations fails when the Rayleigh friction coefficient is much smaller than the Coriolis parameter, and that this failure is enhanced when the width of the forcing is a small fraction of the Rossby radius.

By comparing the solution with a lid with the solution with a free surface, we have shown that the nonlinear solution with a lid overestimates the geopotential for low values of the friction coefficient, and it underestimates the geopotential for large values of the friction coefficient, but the error rapidly decreases when the upper layer becomes deeper than the lower layer. As a practical rule, we can say that the rigid lid can be adopted when the depth of the upper layer is twice the depth of the lower layer, or deeper.

The results presented are relevant for sea-land breeze flows and for cold pool outflows. Further applications of the method developed in this paper should include the ambient stratification, and the effects related to the presence of an ambient wind. Other interesting

developments are the study of the behavior of these currents in a β -plane, and in the presence of a sloping terrain. In addition, the approach presented in this paper can be used for studying the behavior of a current in an axisymmetric system.

Our approach can be also used for ocean flows, for deep water spreading on the ocean floor, for river flows in the estuaries, and for many other shallow flows in nature or in laboratory. This can be done by adopting the appropriate values of the parameters, and by posing the correct boundary conditions.

Acknowledgments.

Authors are grateful to NIWA for kind hospitality and financial support through New Zealand Foundation for Research and Technology Project NIWA-CO1X0701. We are also grateful to the two reviewers for their contribution in improving the manuscript. This research was partially funded by the Project TEMPIO of the Italian Ministry of Agriculture and by the Italian CNR Short Term Mobility Programme.

REFERENCES

- Apel J.R., 1987: *Principles of ocean physics*. Academic Press, New York, 634 pp.
- Baldi M., G.A. Dalu, and R.A. Pielke Sr, 2008: Vertical Velocities and Available Potential Energy Generated by Landscape Variability. Theory. *J. Appl. Met. Clim.*, **47(2)**, 397-410.
- Benjamin T.B., 1968: Gravity current and related phenomena. *J. Fluid Mech.*, **31**, 209-248.
- Dalu G.A. and R.A. Pielke, 1993: Vertical heat fluxes generated by mesoscale atmospheric flow induced by thermal inhomogeneities in the PBL. *J. Atmos. Sci.*, **50**, 919-926.
- Darby L.S., R.M. Banta, and R.A. Pielke Sr, 2002: Comparisons between mesoscale model terrain sensitivity studies and doppler lidar measurements of the sea breeze at Monterey Bay. *Mon. Wea. Rev.*, **130**, 2813-2838.
- Fujita T., 1959: Precipitation and cold air production in mesoscale thunderstorm systems, *J. Met.*, **16**, pp. 454-466.
- Gill A.E., 1980: Some simple solutions for heat-induced tropical circulation. *Quart. J. Roy. Meteor. Soc.*, **106**, 447-462.
- Gill A.E., 1982: *Atmosphere and ocean dynamics*. Academic Press, New York, 662 pp.
- Griffiths R.W., 1986: Gravity currents in rotating systems. *Ann. Rev. Fluid Mech.*, **15**, 59-89.
- Haertel P.T. and R.H. Johnson, S.N. Tulich, 2001: Some simple simulations of thunderstorm outflow, *J. Atmos. Sci.*, **58**, 504-516.
- Hacker J.N. and P.F. Linden, 2002: Gravity currents in rotating channels. Part 1. Steady state theory. *J. Fluid Mech.*, **457**, 295-324.

- Hogg A.J., 2006: Lock-release gravity currents and dam-break flows. *J. Fluid Mech.*, **569**, 61-87.
- Huppert H.E., 2006: Gravity currents: a personal perspective. *J. Fluid Mech.*, **554**, 299-322.
- Huppert H. E. and J.E. Simpson, 1980: The slumping of gravity currents. *J. Fluid Mech.* **99**, 785-799.
- von Kármán T., 1940: The engineer grapples with nonlinear problems. *Bull. Am. Math. Soc.*, **46**, 615-683.
- Liu C.H. and M. W. Moncrieff, 2000: Simulated density currents in idealized stratified environments, *Mon. Wea. Rev.*, **128**, 1420-1437
- Martin J.R. and G.F. Lane-Serff, 2005: Rotating gravity currents. Part 1. Energy loss theory. *J. Fluid Mech.*, **522**, 35-62.
- Martin J.R., D.A. Smeed, and G.F. Lane-Serff, 2005: Rotating gravity currents. Part 2. Potential vorticity theory, *J. Fluid Mech.*, **522**, 63-89.
- Matsuno T., 1966. Quasi-geostrophic motions in the equatorial area. *J. Meteorol. Soc. Jpn*, **44**, 25-43.
- Mizuta G. and A. Masuda, 2003: An application of a diffusive reduced-gravity model to deep circulation above various forms of bottom topography. *J. Phys. Ocean.*, **33**, 451-464
- Moncrieff M.W. and W.K. So, 1989: An hydrodynamical theory of conservative bounded density currents. *J. Fluid Mech.*, **198**, 177-197.
- Moncrieff M.W. and C.H. Liu, 1999: Convection initiation by density currents: role of convergence, shear, and dynamical organization, *Mon. Wea. Rev.*, **127**, 2455-2464
- Pedlosky J., 1987: *Geophysical Fluid Dynamics*. Springer-Verlag, New York, 710 pp.

Pielke R.A. Sr, 2002: *Mesoscale meteorological modeling*. 2nd edition. Academic Press, San Diego, 676 pp.

Polvani L.M. and A.H. Sobel, 2002: The Hadley circulation and the weak temperature gradient approximation. *J. Atmos. Sci.*, **59**, 1744-1752.

Potter D., 1973: *Computational Physics*. John Wiley and Sons, London, 315 pp.

Rottman J. W. and J.E. Simpson, 1983: Gravity currents produced by instantaneous releases of a heavy fluid in a rectangular channel. *J. Fluid Mech.*, **135**, 95-110

Rotunno R., 1983: On the linear theory of land and sea breeze. *J. Atmos. Sci.*, **40**, 1999-2009.

Segal M. and R. W. Arritt, 1992: Nonclassical mesoscale circulations caused by surface sensible heat-flux gradients, *Bull. Amer. Meteor. Soc.*, **73**, 1593-1604.

Seitter K.L., 1986: A numerical study of atmospheric density current motion including the effects of condensation, *J. Atmos. Sci.*, **43**, 3068-3076

Simpson J.E., 1982: Gravity currents in the laboratory, atmosphere, and ocean. *Ann. Rev. Fluid Mech.*, **14**, 213-234.

Simpson J.E., 1994: *Sea breeze and local winds*. Cambridge University Press, UK, 248 pp.

Sobel N. and Bretherton F.P. 2000: Modeling tropical precipitation in a single column. *J. Climate*, **13**, 4378-4392.

Sobel N. and L.M. Polvani, 2001: The weak temperature gradient approximation and balanced tropical moisture waves. *J. Atmos. Sci.*, **58**, 3650-3665.

Thomas P.J. and P.F. Linden, 2007: Rotating gravity currents: small-scale and large-scale laboratory experiments and a geostrophic model. *J. Fluid Mech.*, **578**, 35-65.

Tompkins A.M., 2001: Organization of tropical convection in low vertical wind shears: the role of cold pools. *J. Atmos. Sci.*, **52**, 1650-1672.

Ungarish M. and H.E. Huppert, 1998: The effects of rotation on axisymmetric particle-driven gravity currents. *J. Fluid Mech.*, **362**, 17-51.

Ungarish M. and T. Zemach, 2003: On axisymmetric rotating gravity currents: two-layer shallow water and numerical solutions. *J. Fluid Mech.*, **481**, 37-66.

Zwillinger D. 1992 *Handbook of differential equations*. Academic Press, New York, 787 pp.

List of Figures

- 1 The system rotates around the vertical axis with an angular velocity $\omega = \frac{f}{2}$. Layer 1 and layer 2 are dynamically active, and a free surface decouples these two layers from a very deep and motionless layer 3. $H(x) = \bar{H} + \delta H(x)$ is the free surface (thick line), $\delta H(x)$ is its perturbation, and \bar{H} is its unperturbed depth [thin line above $H(x)$]. $h_1(x) = \bar{h}_1 + \delta h_1(x)$ is the envelope of the density current (thick line), $\delta h_1(x)$ is its perturbation, and \bar{h}_1 is its unperturbed depth [thin line below $h_1(x)$]. For static stability $\rho_3 < \rho_2 < \rho_1$ ($\theta_3 > \theta_2 > \theta_1$). 34
- 2 $h_Q(x)$, solid line; $h_1(x)$ envelope of the current in a geostrophic balanced single-layer flow when $f = 10^{-4} \text{ s}^{-1}$, dash-dot line; same as in the previous case but in the presence of friction when $\lambda_1 = 10^{-4} \text{ s}^{-1}$, dash line. 35
- 3 Isopleths of the geopotential relative error of the linear solution as function of the Coriolis parameter and of the Rayleigh friction coefficient; f and λ_1 have been normalized with $f_0 = 10^{-4} \text{ s}^{-1}$. The dimensions of the source are $X_Q = 0.5R_0$ and $\delta h_{Q_0} = 0.25\bar{h}_1$, with $\bar{h}_1 = 1000 \text{ m}$ and $R_0 = 100 \text{ km}$. 36
- 4 Same as Fig. 3, but when $f = f_0 = 10^{-4} \text{ s}^{-1} = \text{const}$, and as function of the Rayleigh friction coefficient and of the width of the forcing $X_Q R_0^{-1}$, keeping the volume of the diabatic perturbation constant, $2 X_Q \delta h_{Q_0} = 0.25 R_0 \bar{h}_1 = \text{const}$. 37
- 5 Isopleths of the runout length $X R_0^{-1}$ as a function of the Rayleigh friction coefficient λ_1 and of the relative depth $\alpha = \frac{\bar{h}_1}{h_2}$, when $f = f_0 = 10^{-4} \text{ s}^{-1} = \text{const}$, and $\lambda_2 = \lambda_1$ solid line, $\lambda_2 = 0.5 \lambda_1$ dash line, and $\lambda_2 = 0.25 \lambda_1$ dot line. 38
- 6 Same as Fig. 5, but isopleths of the linear e -folding distance, $(R_0 \nu)^{-1}$ (see text) 39

- 7 Isopleths of the relative error of the geopotential of the nonlinear solution with a lid as function of the relative depth $\alpha = \frac{\bar{h}_1}{h_2}$ and of the Rayleigh friction coefficient, λ_1 ; $\lambda_2 = \lambda_1$ solid line, $\lambda_2 = 0.5 \lambda_1$ dash line, and $\lambda_2 = 0.25 \lambda_1$ dot line. 40
- 8 Same as Fig. 2, but for a two layer-flow with a free surface. \bar{H} (solid thin line) and $h_Q(x)$ (solid thick line); $h_1(x)$ (thick dash-dot line) and $H(x)$ (thin dash-dot line) in a geostrophic balanced flow; $h_1(x)$ (thick dash line) and $H(x)$ (thin dash line) in the presence of friction, when $f = \lambda_1 = \lambda_2 = 10^{-4} \text{ s}^{-1}$. 41

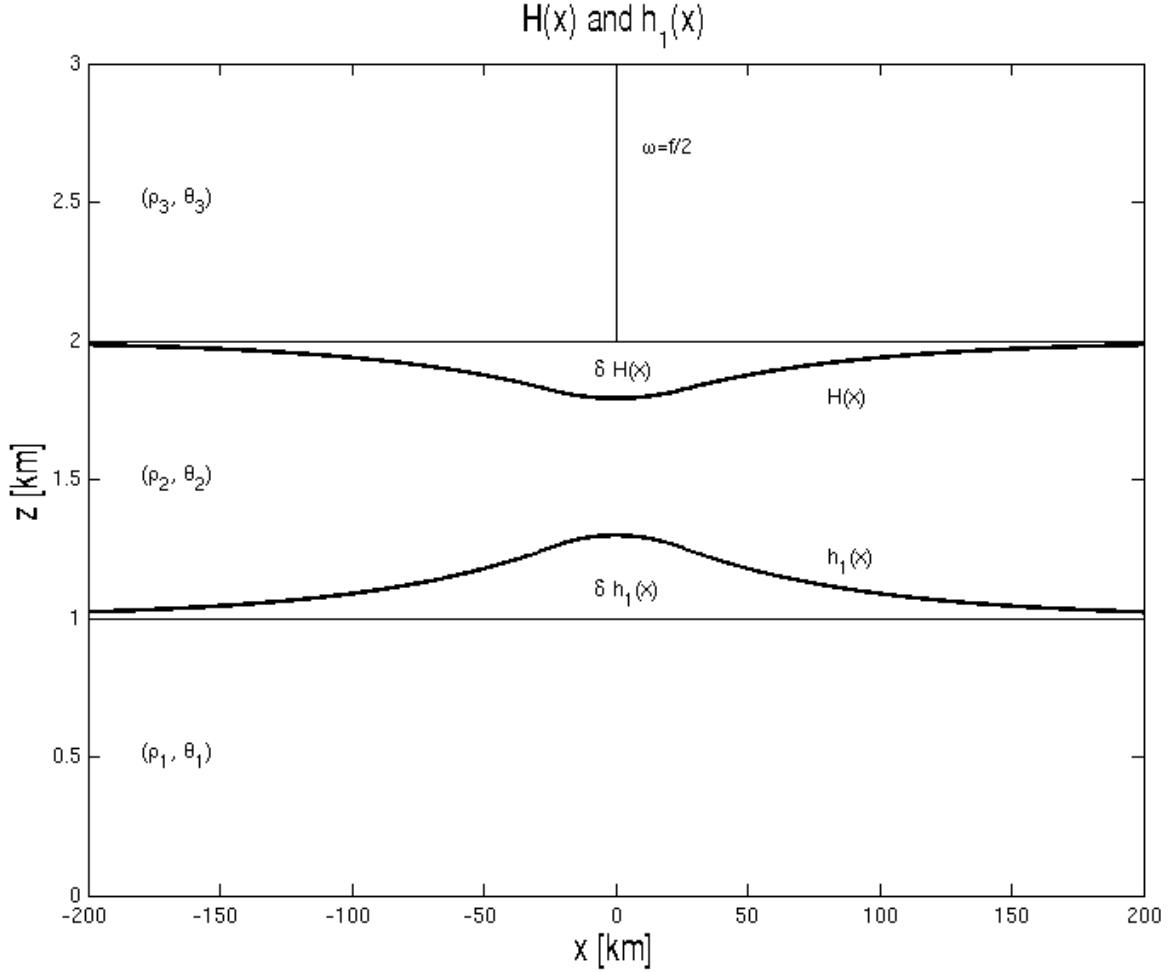


FIG. 1. The system rotates around the vertical axis with an angular velocity $\omega = \frac{f}{2}$. Layer 1 and layer 2 are dynamically active, and a free surface decouples these two layers from a very deep and motionless layer 3. $H(x) = \bar{H} + \delta H(x)$ is the free surface (thick line), $\delta H(x)$ is its perturbation, and \bar{H} is its unperturbed depth [thin line above $H(x)$]. $h_1(x) = \bar{h}_1 + \delta h_1(x)$ is the envelope of the density current (thick line), $\delta h_1(x)$ is its perturbation, and \bar{h}_1 is its unperturbed depth [thin line below $h_1(x)$]. For static stability $\rho_3 < \rho_2 < \rho_1$ ($\theta_3 > \theta_2 > \theta_1$).

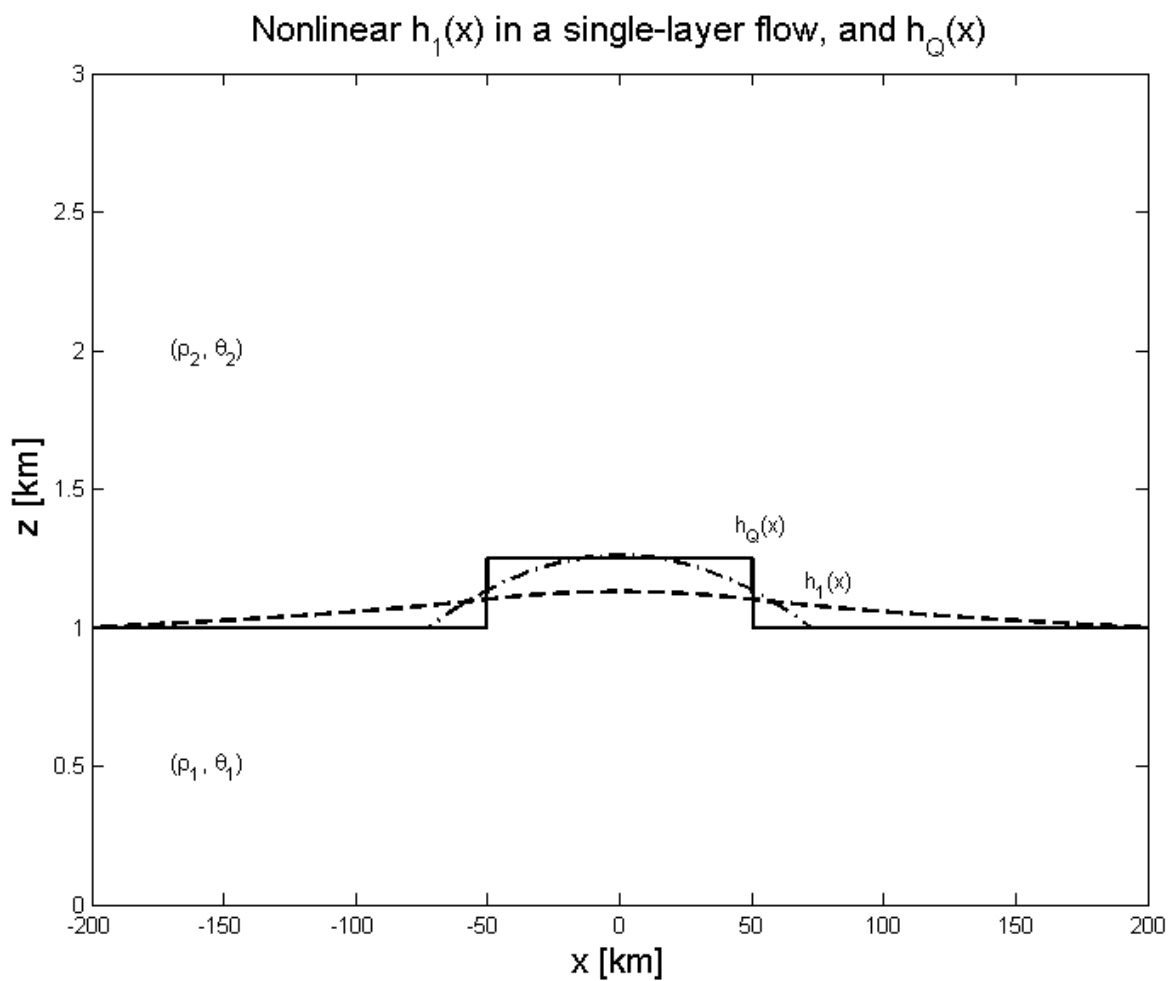


FIG. 2. $h_Q(x)$, solid line; $h_1(x)$ envelope of the current in a geostrophic balanced single-layer flow when $f = 10^{-4} \text{ s}^{-1}$, dash-dot line; same as in the previous case but in the presence of friction when $\lambda_1 = 10^{-4} \text{ s}^{-1}$, dash line.

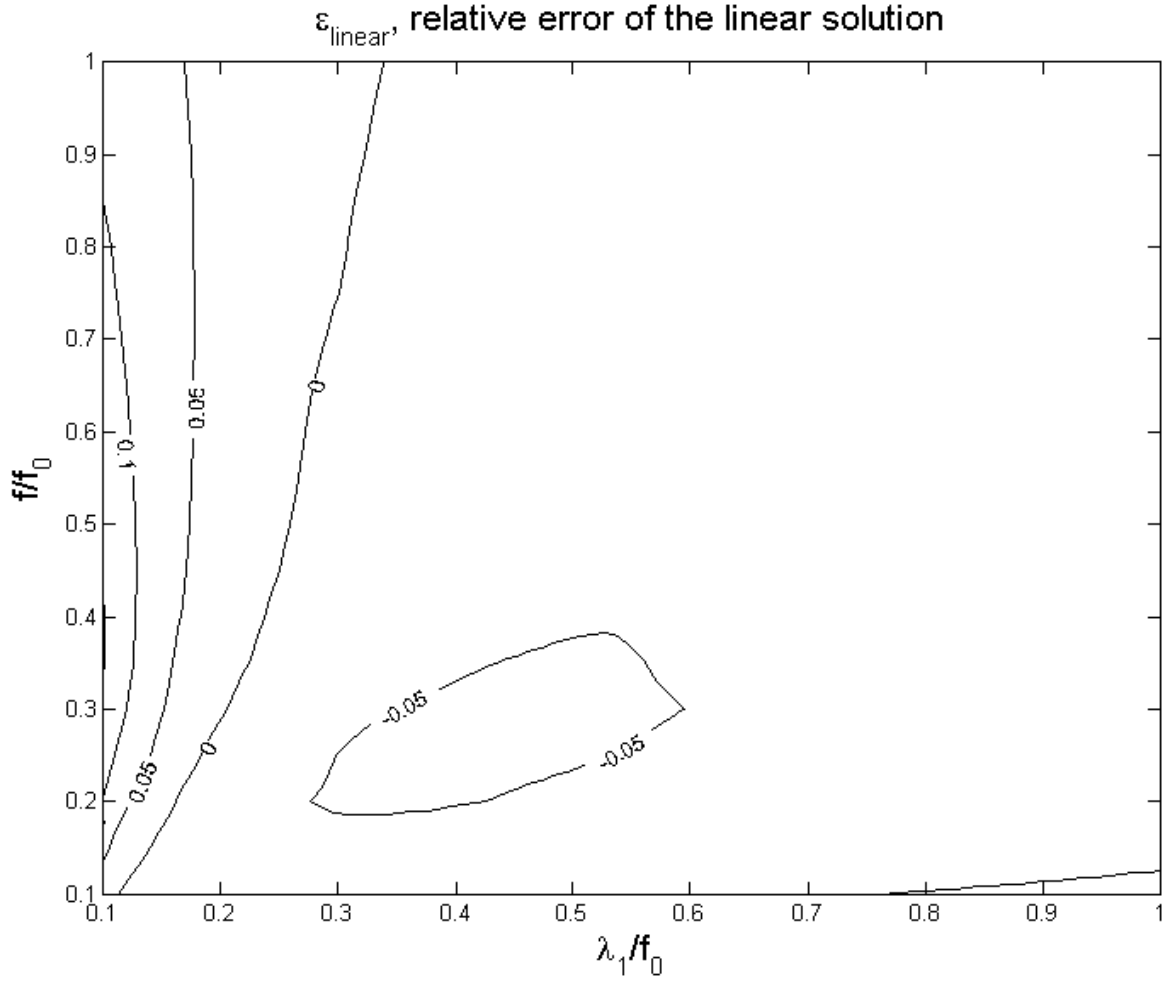


FIG. 3. Isopleths of the geopotential relative error of the linear solution as function of the Coriolis parameter and of the Rayleigh friction coefficient; f and λ_1 have been normalized with $f_0 = 10^{-4} \text{ s}^{-1}$. The dimensions of the source are $X_Q = 0.5R_0$ and $\delta h_{Q_0} = 0.25\bar{h}_1$, with $\bar{h}_1=1000 \text{ m}$ and $R_0=100 \text{ km}$.

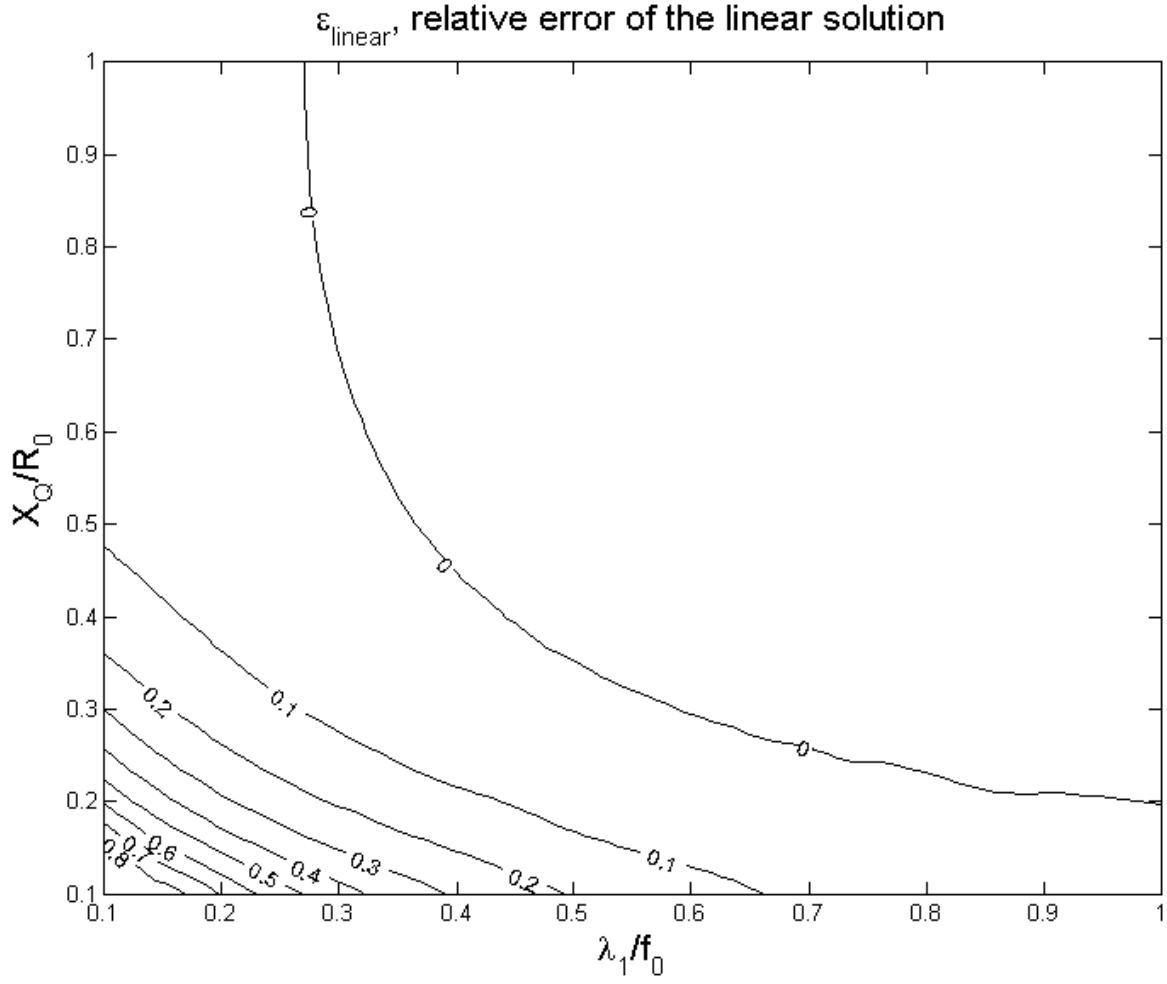


FIG. 4. Same as Fig. 3, but when $f = f_0 = 10^{-4} \text{ s}^{-1} = \text{const}$, and as function of the Rayleigh friction coefficient and of the width of the forcing $X_Q R_0^{-1}$, keeping the volume of the diabatic perturbation constant, $2 X_Q \delta h_{Q_0} = 0.25 R_0 \bar{h}_1 = \text{const}$.

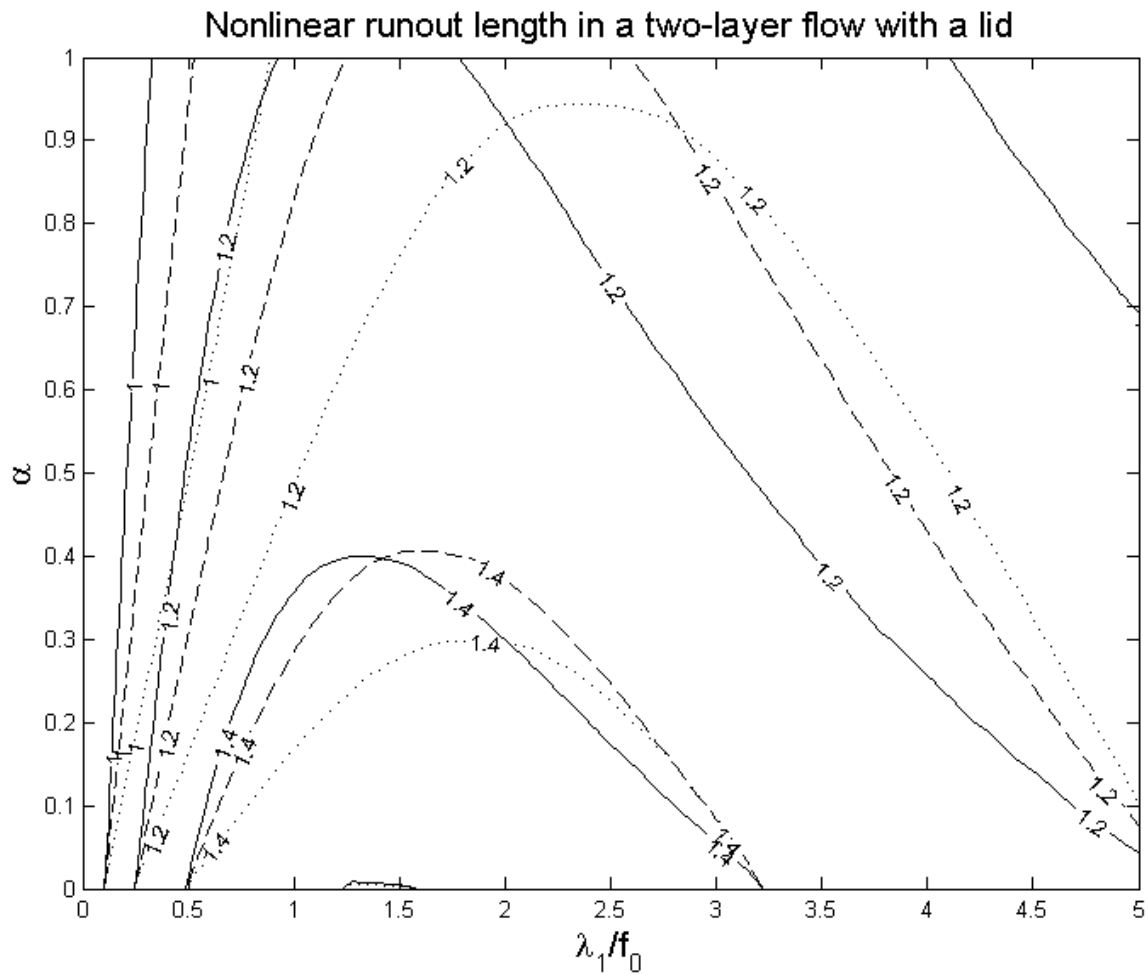


FIG. 5. Isopleths of the runout length XR_0^{-1} as a function of the Rayleigh friction coefficient λ_1 and of the relative depth $\alpha = \frac{h_1}{h_2}$, when $f = f_0 = 10^{-4} \text{ s}^{-1} = \text{const}$, and $\lambda_2 = \lambda_1$ solid line, $\lambda_2 = 0.5 \lambda_1$ dash line, and $\lambda_2 = 0.25 \lambda_1$ dot line.

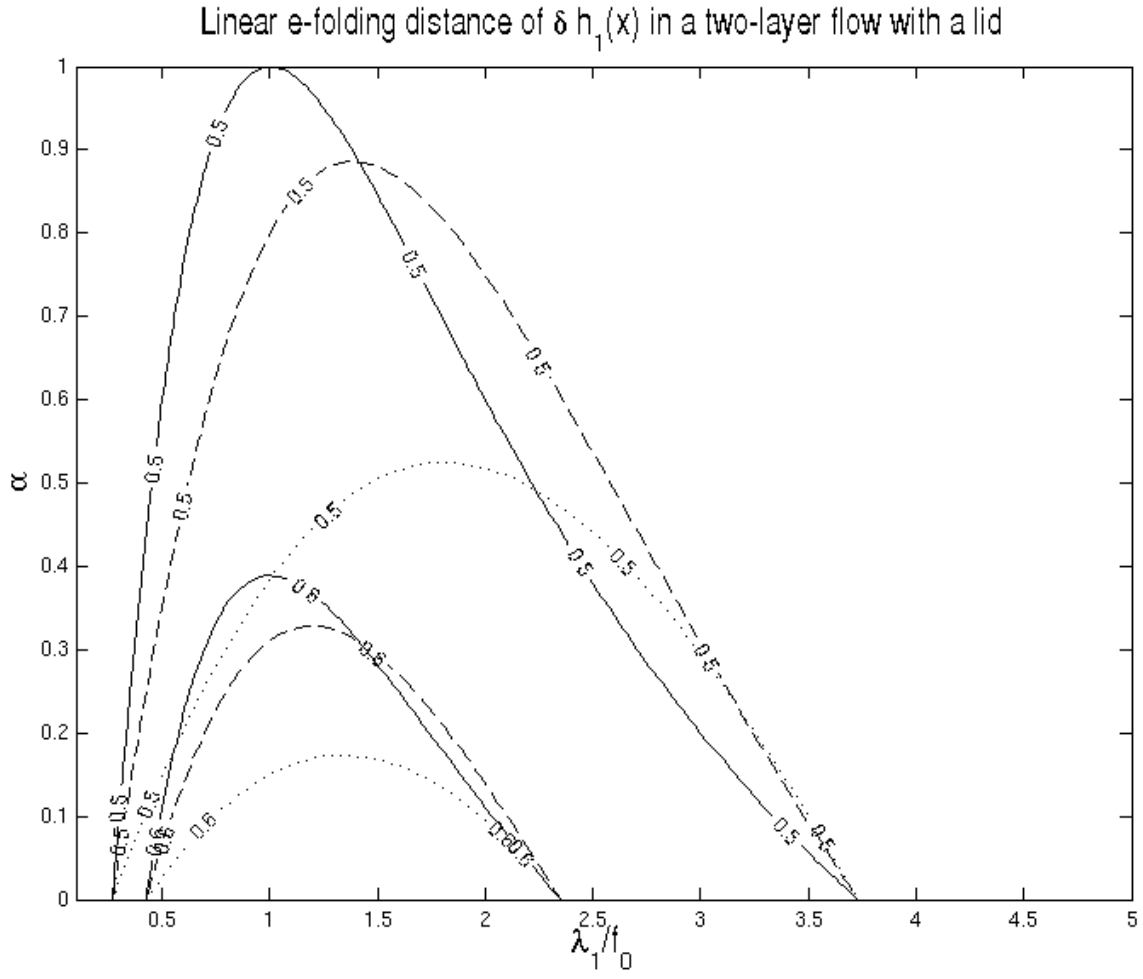


FIG. 6. Same as Fig. 5, but isopleths of the linear e -folding distance, $(R_0\nu)^{-1}$ (see text)

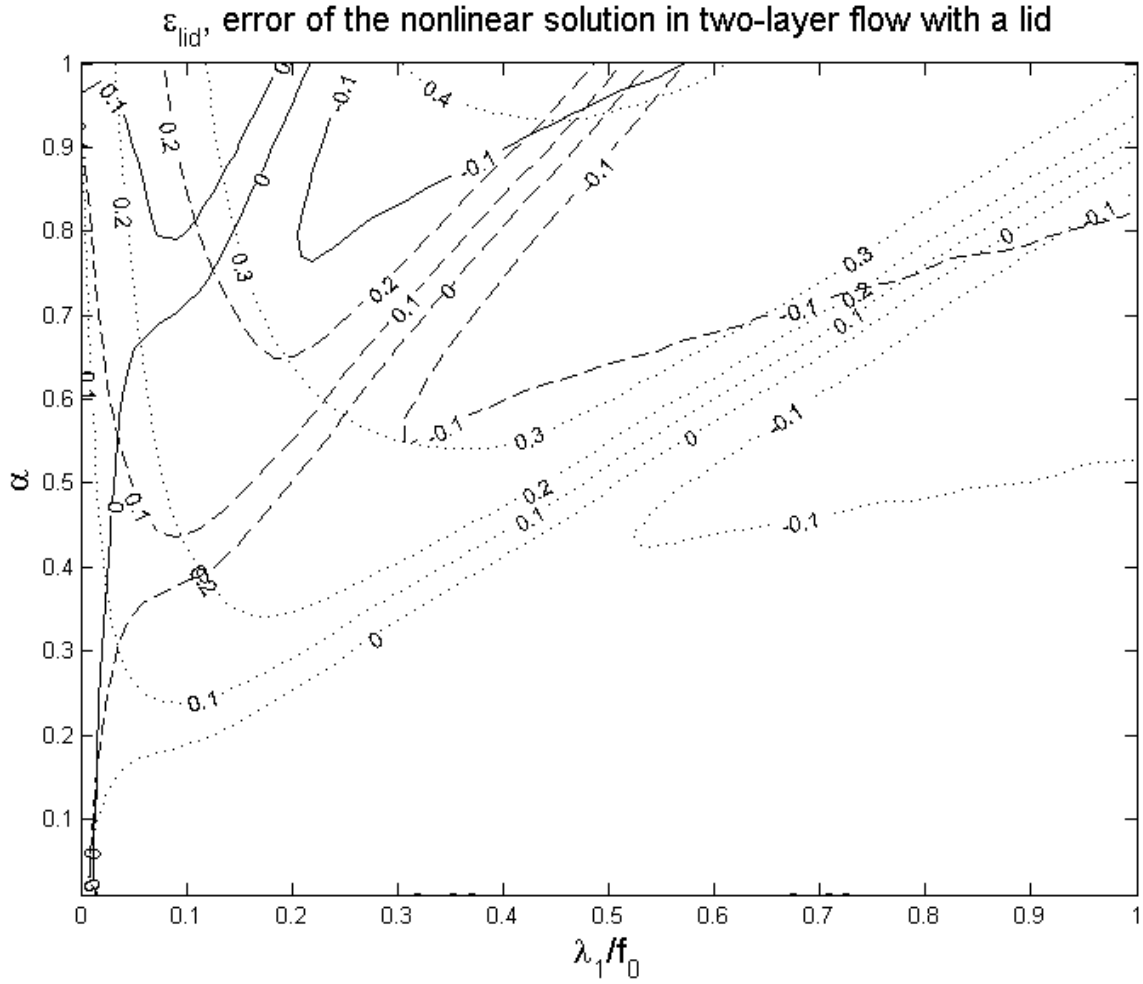


FIG. 7. Isopleths of the relative error of the geopotential of the nonlinear solution with a lid as function of the relative depth $\alpha = \frac{\bar{h}_1}{h_2}$ and of the Rayleigh friction coefficient, λ_1 ; $\lambda_2 = \lambda_1$ solid line, $\lambda_2 = 0.5 \lambda_1$ dash line, and $\lambda_2 = 0.25 \lambda_1$ dot line.

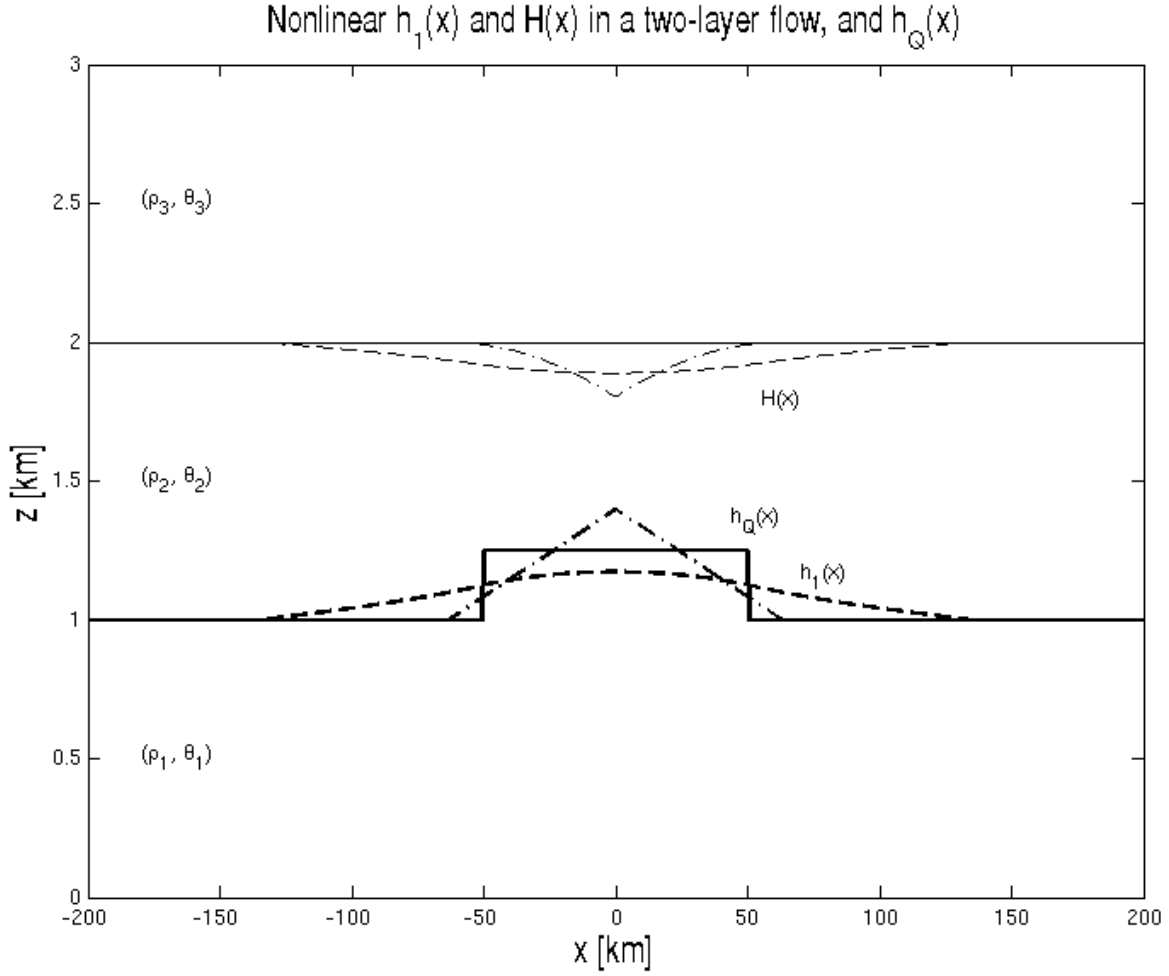


FIG. 8. Same as Fig. 2, but for a two layer-flow with a free surface. \bar{H} (solid thin line) and $h_Q(x)$ (solid thick line); $h_1(x)$ (thick dash-dot line) and $H(x)$ (thin dash-dot line) in a geostrophic balanced flow; $h_1(x)$ (thick dash line) and $H(x)$ (thin dash line) in the presence of friction, when $f = \lambda_1 = \lambda_2 = 10^{-4} \text{ s}^{-1}$.